On the transformation pathways in TRIP/TWIP Ti–12Mo alloy

Bingnan Qian, Lola Lilensten, Jinyong Zhang, Min Yang, Fan Sun, Philippe Vermaut, Frédéric Prima

On the transformation pathways in TRIP/TWIP Ti-12Mo alloy

Bingnan Qian [a], Lola Lilensten [a], Jinyong Zhang [b,c,], Min Yang [d], Fan Sun [a*], Philippe Vermaut [a,e] Frédéric Prima [a]

a., PSL University, Chimie ParisTech, CNRS, Institut de Recherche de Chimie Paris, Paris, France 75005

b. School of Material Science and Engineering, China University of Mining and Technology, Xuzhou, People's Republic of China 221008

c. State Key Laboratory of Solidification Processing, Northwestern Polytechnical University, Xi'an, People's Republic of China 710072

d. School of Automation, Northwestern Polytechnical University, Xi'an, People's Republic of China 710072

e. Sorbonne Universities, UPMC University Paris, UFR926, Paris, France 75005

Corresponding author Email: fan.sun@chimieparistech.psl.eu

This is a post-peer-review, pre-copyedit version of an article published in Materials Science and Engineering A.

The final authenticated version is available online at: https://doi.org/10.1016/j.msea.2021.141672

Keywords: Titanium alloy; Deformation twinning; Martensitic phase transformation.

Abstract:

Diverse pathways of the deformation-induced transformations are investigated in the β-metastable Ti-12Mo alloy displaying combined TWIP ({332}<113>$_\beta$ twinning) and TRIP (stress-induced α″) effects by means of Schmid factor analysis and in-situ microstructural characterizations. Two sets of Schmid factors, for {332}<113>$_\beta$ twinning and stress-induced martensite, are calculated in grains of random orientation under uniaxial tension condition. Using in-situ EBSD characterization under tension, the correspondence is mapped between primary transformation products and the grain orientations. The correspondence results graphically in four grain-orientation domains in the inversed pole figure triangle, being twin-dominated, martensite-dominated, combination of both, and the domain unfavorable for both transformations. It is also

found that the crystallographic partition of the domains, i.e. the selection of transformation pathways with respect to grain orientations, is related to the threshold of Schmid factor for the activation of each transformation and the transformation strain of the corresponding martensite variant. Guided by transformation partition mapping, grains at two special orientations, dominated by stress-induced martensite with-or-without primary $\{332\}\langle 113\rangle_{\beta}$ twinning, are targeted in in-situ microstructural observations to clarify the transformation pathways and the underlying deformation mechanisms. Among the different pathways revealed, experimental evidences are highlighted on the unprecedented formation mechanisms of $\{332\}\langle 113\rangle_{\beta}$ twins assisted by martensite $\{130\}\langle 310\rangle_{\alpha''}$ deformation twinning via two different ways.

1. Introduction

Due to its attractive combination of mechanical properties, the recent family of metastable β titanium alloys with martensitic TRansformation Induced Plasticity (TRIP) and TWinning Induced Plasticity (TWIP) effects has been investigated extensively, leading to great potential applications [1-6]. Combinable deformation mechanisms, mainly including $\{332\}\langle 113\rangle_{\beta}$ twinning, $\{112\}\langle 111\rangle_{\beta}$ twinning, Stress-Induced Martensitic transformation (SIM) (orthorhombic martensite α″), and dislocation glide, have been reported to be responsible for the excellent mechanical properties. Among those mechanisms, $\{332\}\langle 113\rangle_{\beta}$ twinning and SIMα″ have attracted much attention due to their effects on the improvement of strain-hardening rate, mainly as a result of dynamic Hall-Petch effect, and the subsequent large uniform elongation during tensile plastic flow. A large number of researches have been devoted to $\{332\}\langle 113\rangle_{\beta}$ twinning and SIMα″, focusing on the microstructure/mechanical property relationship [1-6], the hierarchical structure [1], the interface/dislocation interactions [2], the modeling of $\{332\}\langle 113\rangle_{\beta}$ twinning [3] and the crystallography of transformation products via

theoretical and experimental methods [4]. Among the reported results, the character of {332}<113>$_\beta$ twinning in the single TWIP Ti alloy has been well understood (Ti15Mo [5], Ti12Mo10Zr [2], Ti13Mo18Zr [6]). The tensile properties can be modelled by predictions from the models proposed by Zhao et al. [3], or based on twinning kinetics and from the viewpoint of solute-solution strengthening effect according to Danard et al. [7]. Details of the crystallography of SIMα″ in metastable Ti-alloys, such as the habit planes and directions [8] [9], and the dependance of the crystal structure to the composition have been well characterized by experimental observations, in good agreement with theoretical predictions. Based on the lattice parameters for Ti-12Mo alloy, which was calculated from the in-situ synchrotron X-ray diffraction results [10], and using $\{111\}_{\alpha''}$ (type I) twinning as the lattice invariant shear [9], the α″ crystallography for the alloys was predicted. Six lattice correspondence variants (CV) could derived from the β to α″[15]. The prediction for one variant of α″ (CV1) is shown in the table 1 as an example. Two habit plane variants, namely CV1 (+) and CV1 (-), were predicted for CV1, which are near to $\{755\}_\beta$ plane. The magnitude of the lattice invariant shear for both habit plane variants are very small, implying that almost no twinning is needed as the lattice invariant shear.

Table 1 Prediction based on the invariant plane strain theory for the α" martensite crystallography in a Ti-12Mo alloy (Lattice parameters were measured under tensile loading at ε=0.024[10])

lattice parameter (Å)	β	α″		
	a_β	$a_{\alpha''}$	$b_{\alpha''}$	$c_{\alpha''}$
	3.27924	3.07871	4.91978	4.63289
Transformation strain of CV1, ε_1	$\begin{pmatrix} -0.06188 & 0 & 0 \\ 0 & 0.03272 & 0.03177 \\ 0 & 0.03177 & 0.03272 \end{pmatrix}_\beta$			
	Solution 1		Solution 2	
variant	CV1(+)		CV1(-)	
Habit plane	(0.6875 0.5212 0.5057) $_\beta$		(0.6976 -0.5218 -0.4910) $_\beta$	

Transformation strain direction	$\begin{pmatrix} -0.7409 \\ 0.4896 \\ 0.4597 \end{pmatrix}$	$\begin{pmatrix} -0.7315 \\ -0.4889 \\ -0.4753 \end{pmatrix}$
lattice invariant shear magnitude	0.0058	0.0058

About the relationship between the {332}<113>$_\beta$ twinning and SIMα″, their intrinsic coupled nature has been studied from a crystallographic point of view in a recent work [4]. The results of Sun et al. [10] have shown that, depending on the local Schmid factor with respect to the external stress, {332}<113>$_\beta$ twinning and SIMα″ could independently nucleate and propagate in the matrix grain, as well as in the twinned β volume (i.e. formation of secondary and tertiary deformation twins and SIMα″). Lilensten et al. have also reported a dependence of the deformation mechanism to the Schmid factor of the grain, which plays a role in the selection of the primary deformation mechanism, SIMα″ or deformation twinning in a TRIP/TWIP alloy, strongly suggesting that not all grains undergo the same deformation path [11]. Focusing on the model TRIP/TWIP Ti-12Mo alloy, Cho et al. [12] proposed a hypothesis regarding the deformation mechanism: SIMα″ can act as a nucleation site for {332}<113>$_\beta$ twinning, and then the SIMα″ could be progressively replaced by {332}<113>$_\beta$ twinning with further loading [12]. Despite numerous attempts, the interplay of the two deformation mechanisms and the transformation pathways occurring in metastable Ti-alloys remain only partially understood, which makes it difficult to predict the mechanical behavior of these materials. Besides, due to the extremely fine deformation features and reversible transformations, studies have to propose an investigation of the deformation mechanisms at the micro-length-scale under in-situ conditions, in order to grab operative mechanisms, or bricks to build an in-depth understanding of these materials. Hence, the aim of present study is to clarify these transformation pathways operating in the β grains of a β-metastable Ti-alloy for

different Schmid factor conditions via Schmid factor calculation coupled with in-situ SEM and ex-situ TEM observations. Ti-12Mo is selected in this study as it is considered in the literature as a model TRIP/TWIP alloy, benefiting from the existing results [10, 12-14].

2. Materials and methods

The Ti-12Mo (wt. %) ingot wase fabricated by vacuum arc-melting using high purity Ti (99.6%) and Mo (99.98%) metals. The alloy was melted at least five times under a high purity argon atmosphere, and annealed in vacuum tubular furnace under 2.0 x 10^{-4} Pa at 1173K for 1.8 ks, followed by water quenching. The quenched ingot was then cold-rolled to 0.5mm sheets, corresponding to a reduction rate of 95%. The cold-rolled sheets were recrystallized at 1173K under high vacuum (2.0 × 10^{-4} Pa) for 1.8 ks and then quenched in water to retain the fully recrystallized β grains with size in the range 50-100 μm. In-situ EBSD tensile samples, with dimensions 40mm × 3mm × 0.5mm, were prepared by electropolishing to obtain a smooth and damage-free surface. Deformation is followed by secondary electron imaging during the loading state and deformation microstructures were analyzed by using in-situ tensile tests coupled with EBSD scans at different strain, performed on a Proxima 100-Micromecha machine, in a field emission gun scanning electron microscope (FEG-SEM ZEISS LEO1530) operating at 20kV and a NORDIF EBSD camera with step size ranging from 0.02 to 0.4 μm. The pixels with a confidence index higher than 0.08 were selected to analyze using the orientation imaging microscopy (OIM) software. A JEOL 2100plus transmission electron microscope (TEM) operating at 200kV was used to be complementary to the superficial analysis of EBSD. Samples for TEM observations were cut from the in-situ EBSD samples to select the grains with specific orientations with respect to the tensile axis, for comparison with the grains studied by EBSD. The

tensile direction was marked on the TEM disks by a straight edge. The disks were polished down from both surfaces to examine the microstructure near the sample core, about 100 microns beneath the surface, by twin-jet electropolishing, using a solution of 4% perchloric acid in methanol, held at about 250 K. The Schmid factor (SF) is defined as: $SF = cos\ \lambda\ cos\ \varphi$, where λ and φ are the angles between the tensile direction and the normal to habit plane (or the twinning plane) and the associate invariant strain direction (or the twinning direction), respectively. The values of λ and φ in each grain were accessed by the EBSD data.

Table 2 Six lattice correspondence variants (CV) derived from β to α″ crystals.

Variant	$[100]_{\alpha''}$	$[010]_{\alpha''}$	$[001]_{\alpha''}$
CV1	$[100]_{\beta}$	$[011]_{\beta}$	$[0\bar{1}1]_{\beta}$
CV2	$[100]_{\beta}$	$[0\bar{1}1]_{\beta}$	$[01\bar{1}]_{\beta}$
CV3	$[010]_{\beta}$	$[101]_{\beta}$	$[10\bar{1}]_{\beta}$
CV4	$[010]_{\beta}$	$[10\bar{1}]_{\beta}$	$[\bar{1}0\bar{1}]_{\beta}$
CV5	$[001]_{\beta}$	$[110]_{\beta}$	$[\bar{1}10]_{\beta}$
CV6	$[001]_{\beta}$	$[\bar{1}10]_{\beta}$	$[1\bar{1}0]_{\beta}$

According to the orientation relationship of β matrix and α″ phase, six variants of SIMα″can be defined and were designated as CV1 to CV6, which are listed in Table 2. The principal strains during the β to α″ transformation is calculated as:

$\eta_1 = (a_{\alpha''} - a_\beta)/ a_\beta$ (Eq.1)

$\eta_2 = (b_{\alpha''} - \sqrt{2}a_\beta)/\sqrt{2}a_\beta$ (Eq.2)

$\eta_3 = (c_{\alpha''} - \sqrt{2}a_\beta)/\sqrt{2}a_\beta$ (Eq.3)

where the lattice parameter of the β phase is a_β and those of SIMα″ are $a_{\alpha''}$, $b_{\alpha''}$ and $c_{\alpha''}$ (table 1). In the normalized β basis, the transformation strain, s_i, resolved on the tensile direction, $[\beta\ ;\ u]$, resulting from the transformation of β phase to the each potential SIMα″

CV_i (i = 1 - 6) can be calculated as:

$s_i = (u\ ;\ \beta)\ (\beta\ \varepsilon_i\ \beta)[\beta\ ;\ u]$. (Eq.4)

where ($\beta\ \varepsilon_i\ \beta$) *is* the transformation tensor for each CV given in ref. [15]. The notation scheme is adopted from the crystallography of martensite transformations introduced by Mackenzie and Bowles [16].

3. Results

3.1 The Schmid factor dependent primary deformation mechanism

About 600 grains of various orientations are analyzed during in-situ tensile tests and their primary deformation mechanism at yielding is characterized by EBSD. Figure 1a shows the EBSD statistical analysis of the primary transformation products in all these grains, originating from the same sample. In this paper, the term “primary” refers to the transformation products directly formed from β matrix at yielding (ε ~ 0.02) and “secondary” refers to the products formed within a primary product. Besides, some special cases observed in this study, such as transformation products that nucleate at the boundary of primary products but grow into the β matrix, are considered to be secondary products since their formation is dependent on the primary products. The orientations of the analyzed β grains are plotted in the inverse pole figure of Figure 1a with respect to the tensile axis. The color code corresponding to different deformation products is adopted. The blue color is attributed to the grains where the primary deformation products are {332}<113>$_\beta$ twinning. The red color highlights the grains showing both {332}<113>$_\beta$ twinning and SIMα″ as primary deformation products. The yellow color is used for grains with only primary SIMα″ transformation. Interestingly, distinct regions clearly appear on the inverse pole figure triangle, suggesting that the transformation products distribution is drastically grain-orientation dependent. The colors are roughly partitioned into three domains, corresponding to their associated

deformation mechanism, which indicates that the deformation mechanisms are not unique even in the same alloy.

In order to interpret the orientation dependence characterized above in terms of criteria for selection of the deformation mechanism, statistical calculation of Schmid factor for random grain orientations is performed for a body-centered cubic (BCC) structure under tensile conditions. The {755}<10 7 7>$_\beta$ habit plane and the associated invariant strain direction [17] are used for Schmid factor calculation according to the agreement between theoretical prediction and EBSD measurement. For the {332}<113>$_\beta$ twinning, the habit plane and twin direction {332}<113>$_\beta$ are used for calculation. For each random grain orientation, the Schmid factor values for every {332}<113>$_\beta$ twinning variants and every SIMα″ variants are calculated and ranked, respectively. The highest values of Schmid factor for each grain orientation among all variants of the two transformation products, {332}<113>$_\beta$ twinning and SIMα″, are drawn in figure 1b and c, respectively.

Three Schmid factor poles of 0.5 are presented by red dots in the inverse pole figure (Figure 1b and c); one corresponds to {332}<113>$_\beta$ twinning (figure 1b), and the other two (Fig. 1c and 1d) correspond to SIMα″ without or with applying transformation strain criterion ($s_i \geq 0$, Eq.4), respectively. The criterion requires that the transformation strain of the SIMα″ variant should be non-negative under applied strain together with non-negative Schmid factor. The lattice strain along the tensile direction, s_i, for each potential SIMα″ variants thus need to be considered. The variant is therefore favorable for activation under tension when both of its Schmid factor and s_i are positive and preferably high [15]. Thus, the Schmid factor inverse pole figure of the variants of SIMα″ with positive value of s_i is shown in the figure 1d. There is only one Schmid factor pole of 0.5 corresponding to SIMα″with positive value of s_i in the inverse pole

figure marked red pot in the figure 1d.

Empirically, the variants with Schmid factor higher than a material-specific threshold value can be considered to be active in metastable Ti alloys where only one transformation mechanism, either {332}<113>$_\beta$ twinning or SIMα″, is operative over the whole material [18]. However, in the TRIP/TWIP Ti alloys, with both mechanisms possibly activated, the Schmid factor threshold of single transformation mechanism proposed above is not sufficient to determine the selected mechanism. The activation of twinning or SIMα″ in a specific grain will thus depend on both the Schmid factor threshold for {332}<113>$_\beta$ twinning and the Schmid factor threshold for SIMα″, that have not been reported in previous literature according to the authors. In this study, we propose a novel method to assess the Schmid factor thresholds of each transformation.

The proposed method is based on the computation of a series of theoretical transformation partition maps for different combinations of Schmid factor thresholds for {332}<113>$_\beta$ twinning and SIMα″. A laboratory made computer program calculates the Schmid factor of all variants of {332}<113>$_\beta$ twinning and those of SIMα″ at a given grain orientation with respect to tensile direction and s_i. Then, the program compares each Schmid factor of {332}<113>$_\beta$ twinning with an arbitrary given Schmid factor threshold for {332}<113>$_\beta$ twinning: the mechanical twinning mechanism is validated or rejected in the grain with the considered orientation, depending on the comparison of its Schmid factor and the defined threshold. The same approach is performed for SIMα″ with $s_i >= 0$ consideration and a corresponding theoretical transformation partition maps is then produced, describing the expected deformation mechanism for each orientation. Comparison of the theoretical transformation partition maps and the experimental one finally allows to find the best match, ultimately providing the Schmid factor threshold for both deformation mechanisms. Practically,

the computation takes thresholds varying between 0.3 and 0.5, with 0.01 steps. For sake of clarity, only selected cases, for Schmid factor thresholds of 0.35, 0.4 and 0.45 for {332}<113>$_\beta$ twinning and Schmid factor thresholds of 0.3, 0.35 and 0.4 for SIMα″ compiled into invers pole figure maps are provided in Figure 1e. The red domain ({332}<113>$_\beta$ twinning+ SIMα") of each transformation partition map, corresponding to a pair of specific Schmid factor thresholds, is unique regarding the size and position. Such unicity allows to study, as suggested above, the Schmid factor thresholds in TRIP/TWIP situation by fitting the given experimental transformation partition maps to the computational ones. For the present Ti-12Mo studied alloy, the situation where the Schmid factor threshold of {332}<113>$_\beta$ twinning equals to 0.4 and the Schmid factor threshold of SIMα″ equals to 0.35, framed in Figure 1e, shows the best agreement between calculated and experimental transformation partition maps (Figure 1a).

By experimental examination of grains with various orientation, and therefore belonging to distinct domains (Figure 1a), the miscellaneous deformed microstructures resulting from different deformation mechanisms and evolution sequence of {332}<113>$_\beta$ twinning and SIMα″ are observed. This results in a large diversity and complexity of the deformation microstructures over the whole sample. The transformation partition maps can therefore be used as a guide to select grains of interests for further investigation on their transformation pathways. For instance, the microstructure of the grains located in the blue and yellow domains (deformation dominated by primary {332}<113>$_\beta$ twinning or SIMα") have been well investigated in many previous researches [1-5] [6]. These results presented that the selections of primary deformation mechanisms in these grains are heterogeneously dominated either by twinning or by SIMα"[11], resulting in the missing of the key information whether the formation of {332}<113>$_\beta$ twinning can be mediated from SIMα". For this reason,

two special grain orientations, I and II marked in Figure 1, are investigated to complete the transformation pathway study between the two mechanisms, where both mechanisms are superior to their Schmid factor thresholds (at Orientation. I) and both of them are inferior to the thresholds (at Orientation. II).

3.2 The orientation dependent pathways to {332}<113>$_\beta$ twinning

At orientation I, the Inverse pole figure and phase maps from a specimen under loading are shown in figure 2a (EBSD scan with keeping the tensile force). Two primary deformation bands form independently, which are identified to be a {332}<113>$_\beta$ twinning (labeled by A in Figure 2a) and a SIMα″ band (labeled by B). The traces of the $(3\ \bar{2}\ 3)_\beta$ and $(5\ 7\ 5)_\beta$ planes are drawn in Figure 2a (white dashed line and black dashed line, respectively), corresponding to the habit plane of each observed bands. It is the first time, according to the knowledge of the authors, that independent formation of primary {332}<113>$_\beta$ twinning and primary SIMα″ is observed simultaneously in the same grain. This can be rationalized by the fact that orientation I is located at the border between the blue region ({332}<113>$_\beta$ twinning dominated) and the red one (combination of {332}<113>$_\beta$ twinning and SIMα″).

Besides, it can be noticed from Figure 2a that a thin layer of α″ is formed during loading at one of the {332}<113>$_\beta$ twinning interface. Similar phenomenon has been reported in previous studies [19], in which focused ion beam (FIB) sampling clarified that it was a superficial α″ layer near the twin interface. It has been proposed to be the evidence of α″-assisted {332}<113>$_\beta$ twinning mechanism [19], although other hypotheses on the origin of this layer could be suggested, such as SIMα″ formed to accommodate the mechanical contrast between the twin and the matrix, similar to what happens with the omega phase [20, 21]. As an extension, in this study, TEM thin foils

are prepared at the core portion of the sample to investigate such interfacial microstructure.

TEM observations were performed on a grain with orientation I, in order to confirm the formation of interfacial α″ and reveal the microstructural details. The bright field image in Figure 2b shows a deformation band in the matrix. The upper region of the band is bordered by another band. The diffraction pattern acquired at the upper interface, pertaining the primary deformation band, the matrix and the interface, allows to identify the primary deformation band as a $\{332\}\langle 113\rangle_{\beta}$ twinning. However, additional diffraction spots that do not belong to the matrix (purple legend in Figure 2c) or the twin (blue legend in Figure 2b) are also visualized. A dark field on one of the spots (red circle (e) in Figure 2b) is provided in Figure 2e, and shows that the interfacial band is made of α″, composed by fine parallel α″ lamellae at $\{332\}\langle 113\rangle_{\beta}$ twinning boundary. The parallel α″ lamellae are separated by the matrix, as highlighted by the dark field of the matrix given in Figure 2f (from the spot (f) shown by a red circle in Figure 2d). The diffraction patterns (figure 2c and figure 2d) taken at the boundary between the $\{332\}\langle 113\rangle_{\beta}$ twinning, α″ and the β matrix and in the β matrix (c and d in Figure 2b), suggest that these α″ lamellae fulfil the classic $(211)_{\beta}$ // $\{110\}_{\alpha''}$ orientation relationship with the β matrix (illustrated in the key diagram in figure 2g). The trace of the habit plane of SIMα″, highlighted by the yellow dotted line in Figure. 2e, corresponds to the $(\bar{7}55)_{\beta}$ trace of β matrix. Due to the low resolution of in-situ EBSD mapping, it is difficult to conclude if the interfacial α″ observed by TEM and by EBSD are the same in microstructure. But the highly organized interfacial α″ lamellae (TEM images in Figure 2) are very different in microstructure than those reported in the literature.

A similar analysis is performed into grains with orientation II (Schmid factor of {332}<113>β twinning is 0.23, Schmid factor of SIM α″is 0.27), located in the difficult transformation domain (near [001]) of Figures 1a (yellow dot in Figure 1a). Deformation microstructure is once again monitored during in-situ tensile tests with EBSD scans at ε=0.02 and ε =0.05 (under loading) and after unloading from ε =0.05. Two SIMα″ bands appear first from the β matrix in the position (marked by the green arrows in figure 3a) where the grain boundary intersects the martensite in adjacent grains at ε=0.02 (Figure 3a). The trace of the habit plane of SIMα″ is parallel to $(7\ 5\ 5)_{\beta}$ trace (marked by orange line in Figure 3a), which can be identified as CV1[17]. The Schmid factor of the six potential SIMα″ in the orientation II as well as the corresponding lattice strain along tensile direction (s_i) are listed in Table 3. The first feature to notice that the CV6 process the highest Schmid factor of SIMα″among the six variants of SIMα″ (0.50), however it is hard to be activated during tensile process since the s_i value of CV6 is negative. At ε =0.05, it is observed that the α″ bands have thickened. The α″ color on the invers pole figure changes from purple to yellow in Figure3b, and crystallographic analysis identifies that these yellow products are secondary $\{130\}\langle 310\rangle_{\alpha''}$ deformation twinning of the primary α″. It should be noticed that two $\{332\}\langle 113\rangle_{\beta}$ twinning bands (marked by gray arrow in Figure 3b) form during the deformation, after the transformation of primary α″, as branches that extend from the main martensite bands into the matrix. The habit plane traces of these $\{332\}\langle 113\rangle_{\beta}$ twinning lie along $(233)_{\beta}$, see black dashed line in Figure 3b, which is about 23° off the habit plane of the primary α″ bands but parallel to the $(130)_{\alpha''}$ twinning plane of the internal $\{130\}\langle 310\rangle_{\alpha''}$ deformation twinning (see purple dashed line in Figure 3b). After unloading from ε =0.5 (Figure 3c), it can be seen that most of the $\{130\}\langle 310\rangle_{\alpha''}$ deformation twinning are reversed to primary α″, strongly suggesting a detwinning

phenomenon. However, part of {130}<310>$_{\alpha''}$ deformation twinning is still preserved after unloading, including those which are aligned with the {332}<113>$_{\beta}$ twinning (marked by black and yellow arrows in figure 3c) and some others (marked by blue arrows in figure 3c) located at the boundaries between the primary α″ bands and the matrix.

Table 3 Transformation lattice strain for each CV along the tensile direction.

Variant	Schmid factor	s_i
CV1	0.27	3.53%
CV2	-0.23	2.98%
CV3	0.27	3.53%
CV4	-0.23	2.98%
CV5	-0.50	-6.14%
CV6	0.50	-6.16%

In order to study the residual {130}<310>$_{\alpha''}$ deformation twinning at the primary SIMα″ boundary, as shown in figure 3c with blue arrows, TEM investigations are performed in a grain with orientation II and the results are shown in Figure 4. The bright field image in Figure 4a provides an overview of the internal microstructure. A large deformation band is identified as orthorhombic SIMα″. The trace of the interface between β matrix and the SIMα″ band (represented in blue in figure 4) is measured close to $(\bar{1}\ 1\ \bar{1})_{\beta}//(\bar{1}\ 2\ 0)_{\alpha''}$ trace, which is one of the classic {hkk}$_{\beta}$ habit plane, but is different from the {755}$_{\beta}$ habit plane observed at the EBSD scale [12-14]. The diffraction pattern and dark field about this interface are shown in figure 4b. From the diffraction pattern, it can be seen that the α″ orientation does not conform to the classical orientation relationship, {211}β //{110}α″, with the β matrix [22].

The bright field image in figure 4a also shows that the martensite band contains internal secondary features. dark field imaging and analysis of the diffraction patterns provided in Figures 4c to figure 4e allow to identify three different types of features.

Dark field image 2 and diffraction patterns 2 in figure 4c show the presence of thin β platelets (variant 2 represented by purple color), with habit plane in the α″ martensite identified as $(7\ 10\ 0)_{\alpha''}$ and $(7\ 5\ 5)_{\beta}$. Secondary $\{110\}\langle 110\rangle_{\alpha''}$ orthorhombic deformation twins are also observed in the martensite, as evidenced in Dark field image 3 and diffraction patterns 3 in figure 4d (represented by pink color). Finally, a second β variant with different orientation from the first ones (yellow color) is found, as illustrated in diffraction patterns 4 and diffraction patterns 4 in figure 4e. As shown in Figure 4, the three dark field images and their corresponding diffraction patterns demonstrate the morphologies and orientation relationships of three different subproducts transformed from the large SIM band (represented by blue color).

4. Discussion

4.1 Schmid factor **-oriented selection of the deformation mechanism**

The computation of transformation partition maps revealed that the invers pole figure triangle is partitioned into three transformation zones and a domain unfavorable for both transformations, each of which corresponds to a deformation mode (figure 1e). This partitioning of deformation induced transformations in Ti-12Mo is originated from the differences of habit planes and shear directions between the $\{332\}\langle 113\rangle_{\beta}$ twinning and SIMα″. The minimal angle is 9.71° between the habit planes of twinning ($\{332\}_{\beta}$) and SIMα″ ($\{755\}_{\beta}$), and the minimal angle between the two shear directions is 19.47°. These geometrical differences result in the polarized distribution of effective Schmid factor (two poles of effective Schmid factor equals to 0.5) (Figure 1b and d). In the experimental invers pole figure (Figure 1a), three distinct domains can be identified, based on the type of activated transformations. This leads to a $\{332\}\langle 113\rangle_{\beta}$ twinning domain, a SIMα″ domain and a $\{332\}\langle 113\rangle_{\beta}$ twinning + SIMα″ domain. As a fact, the transformation partition maps is related to the Schmid factor, the threshold of Schmid

factor for the activation of each transformation, and the transformation strain of the corresponding martensite variant. For example, in a grain belonging to the {332}<113>$_\beta$ twinning domain at yielding point, the Schmid factor of at least one {332}<113>$_\beta$ twinning variant is sufficiently high so that reaching a high enough resolved shear stress initiates the nucleation of such variant to accommodate the local tensile strain. Additionally, in the same grain, the Schmid factor of any variant of SIMα″ is insufficient to reach enough shear stress to activate martensitic transformation. Similar situation happens in the α″ domain, where the grains have at least one operative SIMα″ variant but no operative {332}<113>$_\beta$ twinning variant. Both transformations may become operative, with at least one variant of each, inside the {332}<113>$_\beta$ twinning + SIMα″domain. In addition, the primary deformation products are actually be observed in the unfavorable domain (near [001] pole) where grains possess both lower Schmid factor of {332}<113>$_\beta$ twinning and SIMα″ than each threshold (figure 3). The reason could probably be the stress concentrations due to the deformation incompatibility between the unfavorable grain and its neighbor grains, especially when the neighbors are favorable grains for transformations. Orientation II is of such situation (α″ transmission from neighbor grain marked by green arrows in Fig. 3) among several similar cases examined in this study (not shown in the paper).

4.2 Pathways of twinning and martensitic transformations to accommodate the external and internal stresses

In the view of local microstructure evolution, the deformation starts, in the grains dominated by twinning, with the formation of band-like variants of primary {332}<113>$_\beta$ twinning. The secondary products, SIMα″ and {332}<113>$_\beta$ twinning, occur due to the change of the β orientation by primary twinning operation and also possibly due to the stress concentrations at primary {332}<113>$_\beta$ twinning boundaries

[2, 10, 14]. In the grains governed by twinning and SIMα″, both {332}<113>$_\beta$ twinning and primary SIMα″ can nucleate and grow independently in the same grain to accommodate the external stresses. This is exemplified by the analysis of a grain with orientation I: for this orientation, Schmid factor of {332}<113>$_\beta$ twinning equals to 0.50 and Schmid factor of SIMα″ equals to 0.41, therefore both Schmid factor are above their defined threshold. Indeed, experimental investigation of Figure 2a shows that at the onset of the plastic regime, both mechanisms are triggered in this grain. In the domain theoretically unfavorable for transformations, i.e. near [001] pole, the Schmid factor of the positive SIMα″ variant is always higher than Schmid factor of {332}<113>$_\beta$ twinning. Therefore, when stress concentration occurs at grain boundary due to the deformation incompatibility with respect to neighbor grains, SIMα″ could be activated as the primary deformation prior to {332}<113>$_\beta$ twinning. Nevertheless, {332}<113>$_\beta$ twinning could also be activated as secondary deformation mechanism as shown in Figure 3 and figure 4. Such secondary {332}<113>$_\beta$ twinning in primary martensite mechanism has not be reported in the previous studies of primary SIM α" behaviors in TRIP/TWIP alloys [2] [11], which are usually attributed by reversibility of martensite to beta matrix [11] or massive detwinning of the martensite [2].

Secondary transformations are observed in the primary products or at their interfaces to accommodate local stress. The peculiar α″ martensite at the {332}<113>$_\beta$ twinning boundary (orientation I) exhibits a highly organized structure, in which alternate α″ lamellae of fixed thickness form a regular array. The structure is similar to the well-known transformation twinning microstructure in martensite. In martensite, the function of the array is to obtain an invariant plane strain to accommodate the transformation misfit at martensite/austenite boundary as required by the crystallographic theory of martensite [24]. Analogously, the α″ array at the

{332}<113>$_{\beta}$ twinning could probably fulfill the similar function to accommodate the stress concentration at the twin boundary by highly organized martensitic transformations. It has been well documented that very high stresses are generated in the boundary area of a deformation twin which is confined within an externally stressed parent crystal [25].

In the case of TWIP/TRIP Ti, the highly stressed areas would be at vicinities of grain boundary, {332}<113>$_{\beta}$ twinning boundaries and {130}<310>$_{\alpha''}$ deformation twinning boundaries. The high stress concentration could be related to the primary and secondary transformations. In the case of orientation II, the transformation is very hard to be activated due to its low Schmid factor for both {332}<113>$_{\beta}$ twinning and SIMα″. As show in the Table 3 the activated SIMα″ variant is CV1, and the Schmid factor of CV1 is only 0.27, which is less than the Schmid factor threshold of SIMα″ (0.35, see figure 1e). Even though the resolved shear stress is insufficient to activate this variant of SIMα″ operation according to Schmid factor calculation, the primary α″ band seems to be nucleated at the grain boundary, which would then help to accommodate the stress concentration caused by the intersection of grain boundary and SIMα″ (marked by green arrows in figure 3a) in adjacent grain. The Schmid factor of the variant SIMα″ activated in adjacent grain can be calculated as 0.36, which is higher than the Schmid factor threshold of SIMα″. Similar cases can also be observed in other grains belonging to the difficult transformation domain (near [001] pole, purple area in Figure 1e) in Ti-12Mo alloy. Additionally, the secondary {130}<310>$_{\alpha''}$ deformation twinning in the primary α″ band (see Figure 3) is believed to provide extra shear strain along tensile direction, resulting in the almost fully reorientated parent α″. As observed in fully martensitic Ti alloy under tensile deformation, the reorientation of primary α″ variants are controlled by the local Schmid factor and deformation strain along the tensile

direction [23]. The α″ variant reorientation is known to be reversible after the removal of external stress and sometimes heating the sample and is responsible for the macroscopic superelasticity and shape memory effects. Regarding the detwinning phenomenon observed at Orientation II (Figure 3), the detwinning process is triggered immediately after the unloading, meaning that enough driving force has been stored in the material during the loading step. The driving force could be the stress concentration at the primary α″ interface. At this boundary, the secondary $\{130\}\langle 310\rangle_{\alpha''}$ deformation twinning shears is stopped by the primary α″ habit plane. The two shear planes $(7\ 10\ 0)_{\alpha''}$ for primary SIM α″ transformation and $(1\ 3\ 0)_{\alpha''}$ for secondary twinning intersect each other, leading to strain misfit, between the two variant martensite on each side of the boundary. These stresses arise from the resistance of the β matrix and α″ martensite to the macroscopic change of shape in the twinned volumes [26]. In orientation II of Ti12Mo, the accommodation phenomenon of this interfacial stress, thought to be operative during tensile loading, is the $\{332\}\langle 113\rangle_{\beta}$ twinning branch nucleating at the primary α″ boundary after the $\{130\}\langle 310\rangle_{\alpha''}$ deformation twinning, that then grows into the parent β matrix along a $\{332\}_{\beta}$ plane (please note the portions marked by green arrows in Figure 3b). It is considered a secondary deformation mechanism related to the primary formation of martensite because the $\{332\}\langle 113\rangle_{\beta}$ twinning observed here has a Schmid factor (Schmid factor of $\{332\}\langle 113\rangle_{\beta}$ twinning equals to 0.23) below the Schmid factor for SIMα″ (Schmid factor of SIMα″ equals to 0.27), and the Schmid factor threshold of $\{332\}\langle 113\rangle_{\beta}$ twinning (0.4) is higher than that of SIMα″ (0.35). Correspondingly, the portion of $\{130\}\langle 310\rangle_{\alpha''}$ deformation twinning aligned with this $\{332\}_{\beta}$ plane is preserved after the unloading (note the portions marked by black arrows in Figure 3b). Regarding to the portion of $\{130\}\langle 310\rangle_{\alpha''}$ deformation twinning misaligned to accommodative $\{332\}\langle 113\rangle_{\beta}$ twinning branch, the detwinning happens

probably due to the release of stored backward stress. This leads to the hypothesis that the driving force might be weakened (accommodated) by the formation of {332}<113>$_{\beta}$ twinning branch, which therefore stabilizes the {130}<310>$_{\alpha''}$ deformation twinning, preventing it from detwinning after unloading the external tensile stress. Indeed, the fact that β grain chooses the {332}<113>$_{\beta}$ twinning to accommodate the backward stress is obviously reasonable, because the shear planes and directions are perfectly parallel between the equivalent {130}<310>$_{\alpha''}$ deformation twinning system and {332}<113>$_{\beta}$ twinning system operating in the same β matrix. Furthermore, the {332}<113>$_{\beta}$ twinning contributes to the overall shear strain for the tensile deformation of the grain, even though the resolved shear stress is insufficient to activate such twinning operation according to Schmid factor calculation (Schmid factor of {332}<113>β twinning equals to 0.23, which is lower than 0.4). Nevertheless, the formation of the {332}<113>$_{\beta}$ twinning branches as an extension of {130}<310>$_{\alpha''}$ deformation twinning into β matrix (marked by yellow arrow in figure 3c), or similar cases, have never been reported, according to the authors.

4.3 Pathways of {332}<113>$_{\beta}$ twinning formation via {130} <310>$_{\alpha''}$ deformation twinning in martensite

The situation of accommodation is more complicated in the preserved {130}<310>$_{\alpha''}$ deformation twinning without {332}<113>$_{\beta}$ twinning accommodation (see the portions marked by blue arrows in Figure 3c) in Orientation II. TEM observations reveal a complex secondary microstructure in one of this {130}<310>$_{\alpha''}$ deformation twinning that remains after unloading (Figure 4). The origin of these secondary features was rationalized by reconstructing their orientation relationships and habit planes in a stereographic projection given in Figure 5a along the zone axis and directions (A1 and A2, respectively) of figure 4.

The interface of the observed main α″ band (marked by blue color in figure 4) and β matrix is measured as $(\bar{1}\ 1\ \bar{1})_{\beta}/(1\ \bar{2}\ 0)_{\alpha''}$.(as shown in figure 5a box 1#). From the diffraction pattern (figure 4b) it can be seen the main α″ band has an orientation relationship of $(130)_{\alpha''}//(\bar{3}3\bar{2})_{\beta}$ with β matrix (box 2#), which does not conform the classic orientation relationship to β matrix. This unexpected orientation relationship, compared to the one observed at the meso-scale by EBSD, was interpreted as the following: the β matrix (in red in Figure 5a) first formed primary martensite (marked by green dot in figure 5), with the conventional habit plane $\{5\ 5\ 7\}_{\beta}$. The whole martensitic band then deformed by a $\{130\}\langle 310\rangle_{\alpha''}$ deformation twinning operation, which resulted in an unexpected habit plane and transformed orientation relationship. This band, being then fully a $\{130\}\langle 310\rangle_{\alpha''}$ deformation twinning, is somehow preserved after unloading probably due to the internal microstructure. In it, two variants of β phase and one variant of α″ phase are recorded. The two variants of β phase in the $\{130\}\langle 310\rangle_{\alpha''}$ deformation twinning band, β V1 marked by yellow dots and β V2 marked by purple dots, conform with the classical orientation relationship (box 4# and 6#), $\{211\}_{\beta}//\{110\}_{\alpha''}$, and conventional $\{557\}_{\beta}$ habit plane (box 3# and 7#) with $\{130\}\langle 310\rangle_{\alpha''}$ deformation twinning. Besides, the one variant of α″ conforms a $\{110\}\langle \bar{1}10\rangle_{\alpha''}$ twinning relationship with $\{130\}\langle 310\rangle_{\alpha''}$ deformation twinning (box 5#).

Based on the TEM observations in figure 4, figure 5b and Figure 5c show a schematic illustration about the transformation pathway in the grain with orientation II. Primary SIM α″ appeared first in the deformation process and then $\{130\}\langle 310\rangle_{\alpha''}$ deformation twinning forms inside the SIMα″ until filling the whole martensitic volume, generating a new variant of α″. Part of it is then transformed via $\{110\}_{\alpha''}$ twinning mode.

Additionally, two variants of β phase are formed in the {130}<310>$_{\alpha''}$ deformation twinning needle. Among them, one variant (β V1) shows a {332}<113>$_{\beta}$ twinning orientation relationship with the β matrix while the other variant (β V2) does not conform to any known orientation relationship to the β matrix. It should be noticed that, the {332}<113>$_{\beta}$ twinning (β V1) exhibits a much longer interface trace with the {130}<310>$_{\alpha''}$ deformation twinning martensite than with the β matrix, suggesting that the {332}<113>$_{\beta}$ twinning (β V1) should form from the reverse martensitic transformation from α″ to β phase. This is the first experimental observation that the formation of {332}<113>$_{\beta}$ twinning can be induced by the reverse transformation from {130}<310>$_{\alpha''}$ deformation twinning in Ti-12Mo alloy. Thanks to the formation of {332}<113>$_{\beta}$ twinning (β V1), the habit plane between {332}<113>$_{\beta}$ twinning (β V1) and {130}<310>$_{\alpha''}$ deformation twinning becomes the normal {332}<113>$_{\beta}$ twinning interface (marked by red dashed line in figure 4a), showing deflections along the original trace (7-55)$_{\beta}$ habit plane (marked by yellow dashed line in Figure 4a). However, the rest (marked by blue dashed line in figure 4a) of the interface between the primary twinned α″ needle and the matrix can be identified as (111)$_{\beta}$, which are still far from the ideal lattice invariant configuration ({755}$_{\beta}$ habit plane) between the α″ and β matrix, since the {130}<310>$_{\alpha''}$ deformation twinning is directly in contact with the β matrix without the parent primary α″ as intermediate layer (can be seen in Figure. 4b and outlined in Figure 5c). Based on the observation that the {130}<310>$_{\alpha''}$ deformation twinning is actually preserved with such microstructure, it is thought that all these internal transformations may be responsible for stabilizing the non-lattice-invariant interface, thus inhibiting the detwinning of the {130}<310>$_{\alpha''}$ deformation twinning otherwise observed in EBSD.

5. Conclusion

In this work, we proposed a method to describe and predict the distribution of the primary deformation mechanisms for all the grain orientations in TRIP/TWIP Ti alloys. The proposed method is based on the experimental transformation partition maps and the computation of a series of theoretical transformation partition maps for different combinations of Schmid factor thresholds for {332}<113>$_{\beta}$ twinning and SIMα″. The following main results are obtained.

1. The transformation pathway in Ti12Mo depends on the grain-orientation. The transformation pathways could be partitioned into four orientation domains in the stereographic triangle based on the Schmid factor simulation, leading to "transformation partition maps". They correspond to twin-dominated- or martensite-dominated-deformation or a combination of both or the domain unfavorable for both transformations.
2. The transformation pathways are highly diversified in TRIP/TWIP alloys due to the operations of the two transformations in a cascade manner with respects to the external tensile stress resolved in each grain; to the deformation incompatibility between neighbor grains belonging to different orientation domains; and to the strain-stress misfits at newly formed interfaces by {332}<113>$_{\beta}$ twinning and SIMα″. The transformations are adaptive to the local deformation condition at each grain without a unique pathway.
3. Experimental evidences are highlighted on the unprecedented formation mechanisms of {332}<113>$_{\beta}$ twinning assisted by martensite {130}<310>$_{\alpha''}$ deformation twinning via two different ways.

Acknowledgments:

The work was supported by National Natural Science foundation of China (Grant No. 51601216) and Fund of State Key Lab of Advanced Metals and Materials, University of Science and Technology Beijing (Grant No.: 2019-ZD03). Mr. Bingnan Qian is sponsored by the China Scholarship Council.

Reference

[1] J. Zhang, Y. Fu, Y. Wu, B. Qian, Z. Chen, A. Inoue, Y. Wu, Y. Yang, F. Sun, J. Li, Hierarchical {332}< 113> twinning in a metastable β Ti-alloy showing tolerance to strain localization, Mater. Res. Lett. 8 (2020) 247-253. https://doi.org/10.1080/21663831.2020.1745920.

[2] B. Qian, J. Zhang, Y. Fu, F. Sun, Y. Wu, J. Cheng, P. Vermaut, F. Prima, In-situ microstructural investigations of the TRIP-to-TWIP evolution in Ti-Mo-Zr alloys as a function of Zr concentration., J. Mater. Sci. Technol. 65 (2020) 228-237. https://doi.org/10.1016/j.jmst.2020.04.078.

[3] G.H. Zhao, X.Z. Liang, B. Kim, P.E.J. Rivera-Díaz-del-Castillo, Modelling strengthening mechanisms in beta-type Ti alloys, Mater. Sci. Eng. A 756 (2019) 156-160. https://doi.org/10.1016/j.msea.2019.04.027.

[4] Y. Gao, Y. Zheng, H. Fraser, Y. Wang, Intrinsic coupling between twinning plasticity and transformation plasticity in metastable β Ti-alloys: A symmetry and pathway analysis, Acta Mater. 196 (2020) 488-504. https://doi.org/10.1016/j.actamat.2020.07.020.

[5] X. Min, X. Chen, S. Emura, K. Tsuchiya, Mechanism of twinning-induced plasticity in β-type Ti–15Mo alloy, Scr. Mater. 69 (2013) 393-396. https://doi.org/10.1016/j.scriptamat.2013.05.027.

[6] J. Zhang, F. Sun, Z. Chen, Y. Yang, B. Shen, J. Li, F. Prima, Strong and ductile beta

Ti–18Zr–13Mo alloy with multimodal twinning, Mater. Res. Lett. 7 (2019) 251-257. https://doi.org/10.1080/21663831.2019.1595763.

[7] Y. Danard, F. Sun, T. Gloriant, I.F. Von Thüngen, M. Piellard, F. Prima, The Influence of Twinning on the Strain–Hardenability in TRIP/TWIP Titanium Alloys: Role of Solute–Solution Strengthening, Front. Mater.7 (2020)240. https://doi.org/10.3389/fmats.2020.00240.

[8] P. Gaunt, J.W. Christian, The crystallography of the β-α transformation in zirconium and in two titanium-molybdenum alloys, Acta Metall. 7 (1959) 534-543. https://doi.org/10.1016/0001-6160(59)90189-0.

[9] T. Inamura, J.I. Kim, H.Y. Kim, H. Hosoda, K. Wakashima, S. Miyazaki, Composition dependent crystallography of α″-martensite in Ti–Nb-based β-titanium alloy, Philos. Mag. 87 (2007) 3325-3350. https://doi.org/10.1080/14786430601003874.

[10] F. Sun, J.Y. Zhang, M. Marteleur, T. Gloriant, P. Vermaut, D. Laillé, P. Castany, C. Curfs, P.J. Jacques, F. Prima, Investigation of early stage deformation mechanisms in a metastable β titanium alloy showing combined twinning-induced plasticity and transformation-induced plasticity effects, Acta Mater. 61 (2013) 6406-6417. https://doi.org/10.1016/j.actamat.2013.07.019.

[11] L. Lilensten, Y. Danard, C. Brozek, S. Mantri, P. Castany, T. Gloriant, P. Vermaut, F. Sun, R. Banerjee, F. Prima, On the heterogeneous nature of deformation in a strain-transformable beta metastable Ti-V-Cr-Al alloy, Acta Mater. 162 (2019) 268-276. https://doi.org/10.1016/j.actamat.2018.10.003.

[12] K. Cho, R. Morioka, S. Harjo, T. Kawasaki, H.Y. Yasuda, Study on formation mechanism of {332}< 113> deformation twinning in metastable β-type Ti alloy focusing on stress-induced α ″ martensite phase, Scr. Mater. 177 (2020)106-111.

https://doi.org/10.1016/j.scriptamat.2019.10.011.

[13] W. Zhang, Y. Liu, H. Wu, M. Song, T. Zhang, X. Lan, T. Yao, Elastic modulus of phases in Ti–Mo alloys, Mater. Charact. 106 (2015) 302-307. https://doi.org/10.1016/j.matchar.2015.06.008.

[14] S.A. Mantri, F. Sun, D. Choudhuri, T. Alam, B. Gwalani, F. Prima, R. Banerjee, Deformation Induced Hierarchical Twinning Coupled with omega transformation in a Metastable β-ti Alloy, Sci. Rep. 9(2019) 1-8. https://doi.org/10.1038/s41598-018-37865-0.

[15] E. Bertrand, P. Castany, Y. Yang, E. Menou, T. Gloriant, Deformation twinning in the full-α ″martensitic Ti–25Ta–20Nb shape memory alloy, Acta Mater. 105 (2016) 94-103. https://doi.org/10.1016/j.actamat.2015.12.001.

[16] J.S. Bowles, J.K. Mackenzie, The crystallography of martensite transformations I, Acta metal. 2 (1954) 129-137. https://doi.org/10.1016/0001-6160(54)90102-9.

[17] Y.W. Chai, H.Y. Kim, H. Hosoda, S. Miyazaki, Self-accommodation in Ti–Nb shape memory alloys, Acta Mater. 57 (2009) 4054-4064. https://doi.org/10.1016/j.actamat.2009.04.051.

[18] E. Bertrand, P. Castany, I. Péron, T. Gloriant, Twinning system selection in a metastable β-titanium alloy by Schmid factor analysis, Scr. Mater. 64 (2011) 1110-1113. https://doi.org/10.1016/j.scriptamat.2011.02.033.

[19] M.J. Lai, C.C. Tasan, D. Raabe, On the mechanism of {332} twinning in metastable β titanium alloys, Acta Mater. 111 (2016) 173-186. https://doi.org/10.1016/j.actamat.2016.03.040.

[20] Y. Yang, P. Castany, E. Bertrand, M. Cornen, J.X. Lin, T. Gloriant, Stress release-induced interfacial twin boundary ω phase formation in a β type Ti-based single crystal displaying stress-induced α" martensitic transformation, Acta Mater. 149

(2018) 97-107. https://doi.org/10.1016/j.actamat.2018.02.036.

[21] Q. Chen, S. Ma, S. Wang, The Nucleation and the Intrinsic Microstructure Evolution of Martensite from 332⟨ 113⟩ β Twin Boundary in β Titanium: First-Principles Calculations, Metals 9 (2019) 1202. https://doi.org/10.3390/met9111202.

[22] H.Y. Kim, Y. Ikehara, J.I. Kim, H. Hosoda, S. Miyazaki, Martensitic transformation, shape memory effect and superelasticity of Ti–Nb binary alloys, Acta Mater. 54 (2006) 2419-2429. https://doi.org/10.1016/j.actamat.2006.01.019.

[23] X.H. Min, S. Emura, T. Nishimura, K. Tsuchiya, K. Tsuzaki, Microstructure, tensile deformation mode and crevice corrosion resistance in Ti–10Mo–xFe alloys, Materials Mater. Sci. Eng. A 527 (2010) 5499-5506. https://doi.org/10.1016/j.msea.2010.06.016.

[24] D. Banerjee, J.C. Williams, Perspectives on titanium science and technology, Acta Mater 61 (2013) 844-879. https://doi.org/10.1016/j.actamat.2012.10.043.

[25] J.W. Christian, S. Mahajan, Deformation twinning, Progress in materials science 39 (1995) 1-157. https://doi.org/10.1016/0079-6425(94)00007-7.

[26] J.W. Christian, The theory of transformations in metals and alloys, Newnes (2002). https://doi.org/10.1016/0079-6425(94)00007-7.

Figures:

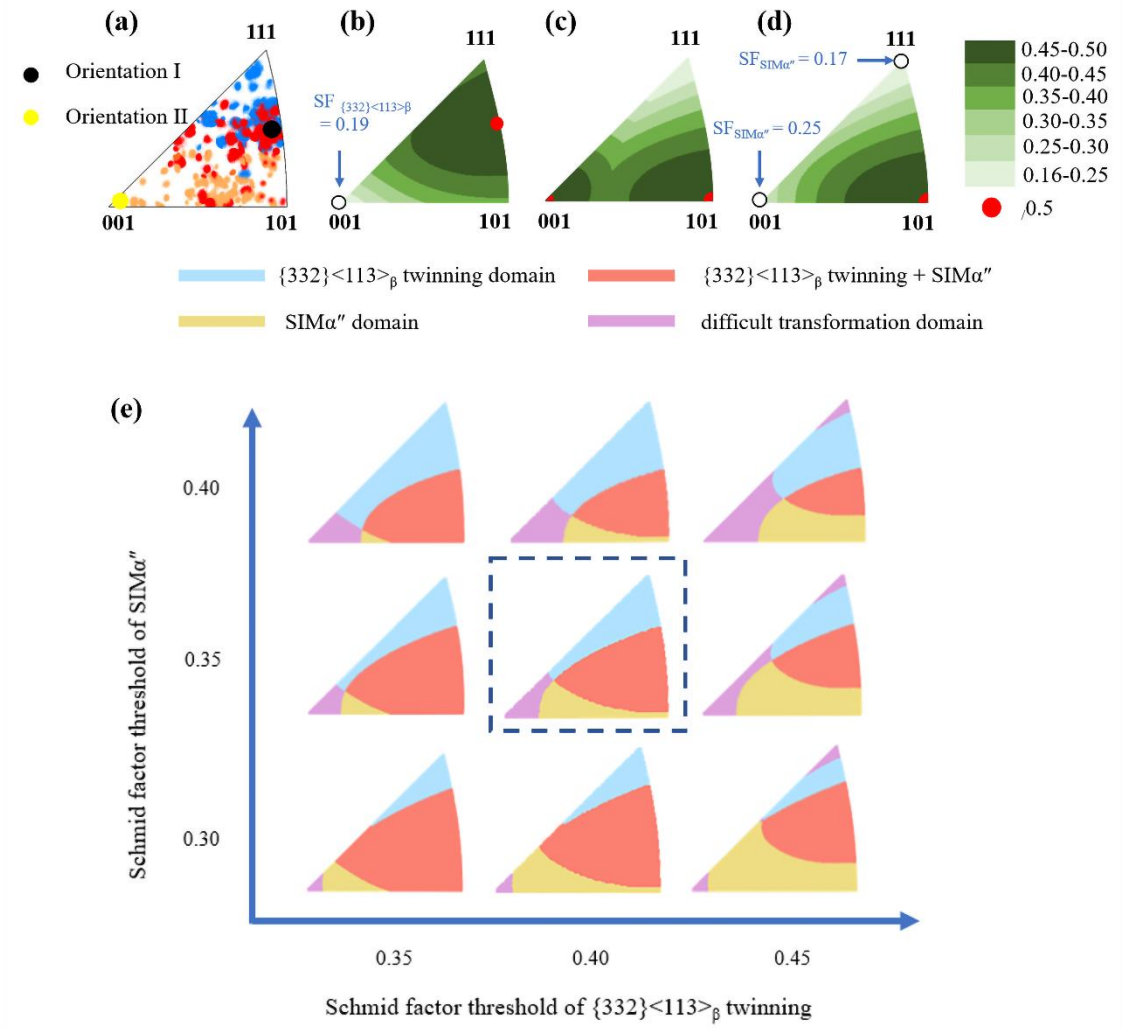

Figure 1: (a) Experimental transformation partition map : Experimental Invers pole figure of the statistic of the primary deformation products in different Ti-12Mo grains by in-situ EBSD under tensile strain (ε =0.02); (b~d) invers pole figure showing the distribution of the highest SF of {332}<113>β twinning(b) ,all variant of SIMα″(c), and the variant of SIMα″ with positive value of ε_i under tensile deformation; (e) theoretical transformation partition maps: invers pole figures of the calculation of the orientation domains as a function of the combinations of threshold SFs. The one marked by a dash square conforms the domain distribution observed experimentally in (a). The normal direction of invers pole figures is along the tensile direction.

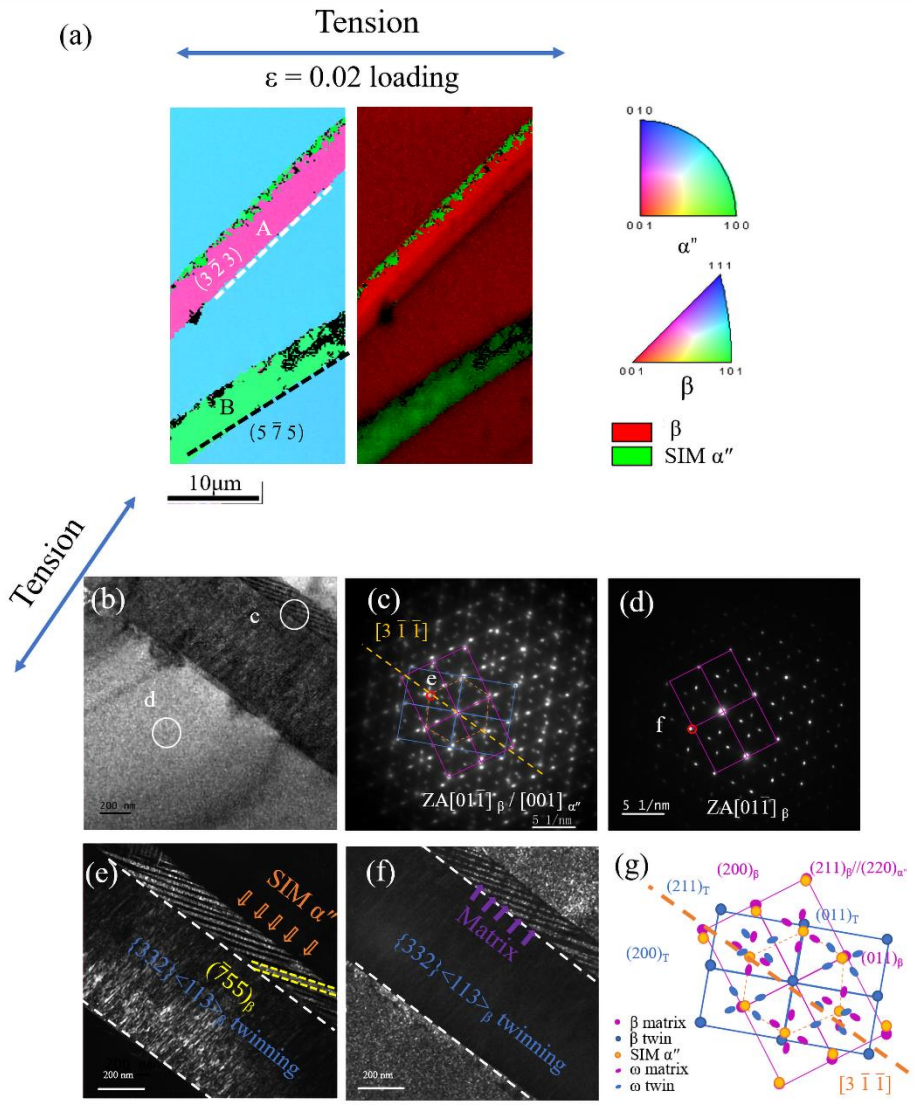

Figure 2. EBSD and TEM investigations at grains with orientation I: (a) invers pole figure maps and phase + IQ maps of the deformed sample taken at ε=0.02 (holding tensile stress); (b) bright-field image of a {332}<113> with interfacial SIMα″ in sample taken at ε=0.05 (unloading), (c-d) diffraction pattern taken from region indicated by circle in (b), (e) and (f) corresponding dark-field images of one variant of SIMα″and of the β matrix, respectively, and (g) key diagrams corresponding to the diffraction pattern in (c).

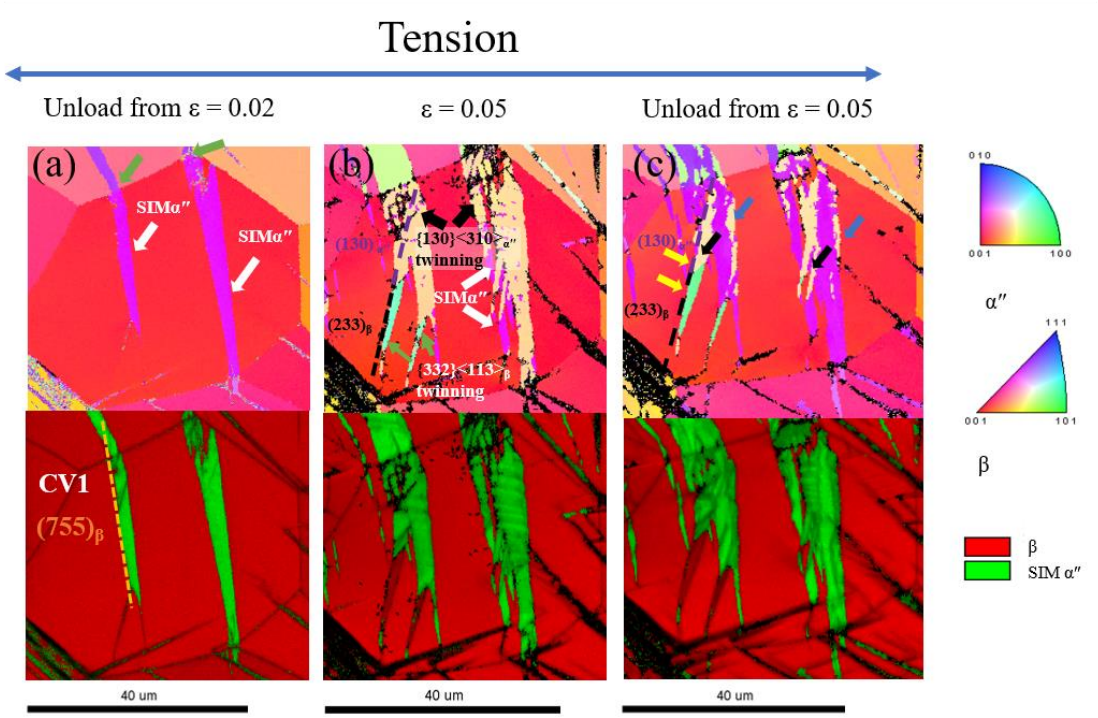

Figure 3. invers pole figure maps and phase + IQ maps of grain with orientation II taken from the same region at strain steps of (a) ε=0.02, (b) 0.05 (holding tensile stress), and (c) 0.05 (stress released).

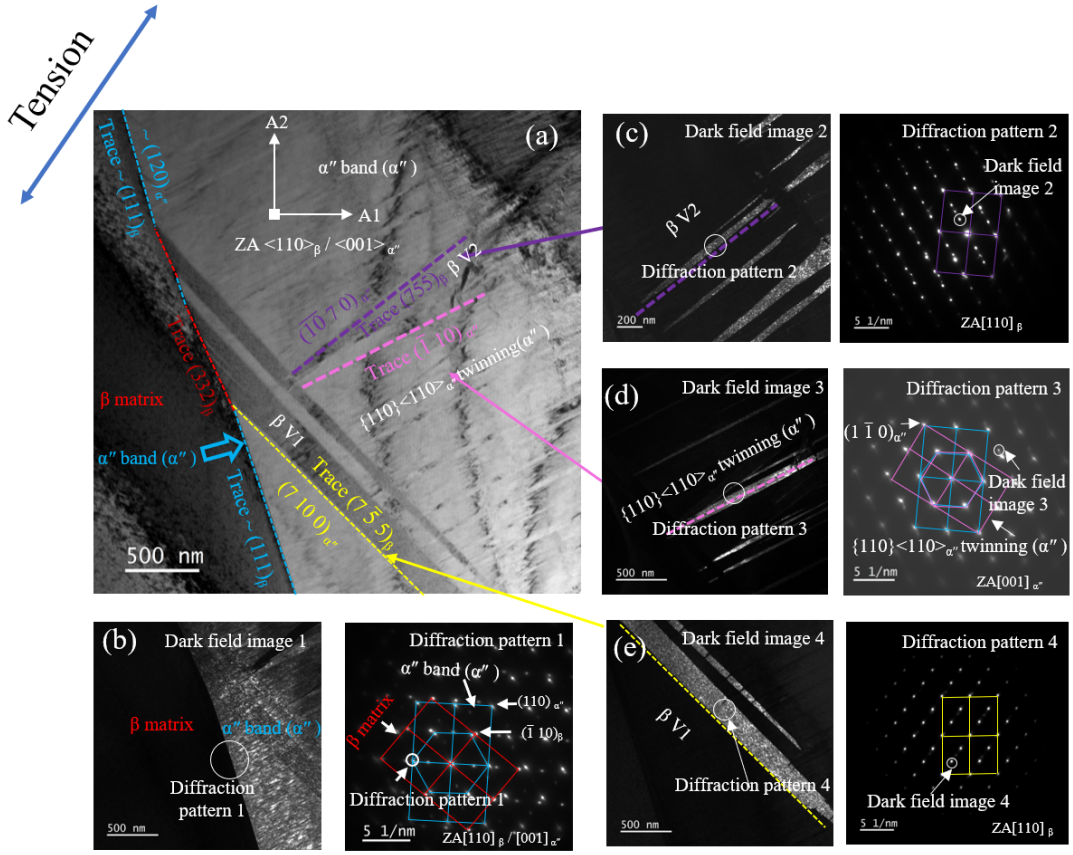

Figure 4 TEM observations of a grain with orientation II in a specimen strained to 0.05 and unloaded. Micrographs of (a) bright field image, (b-e) dark field images and their corresponding diffraction patterns (DP) associated by arrows to the locations of the interfaces.

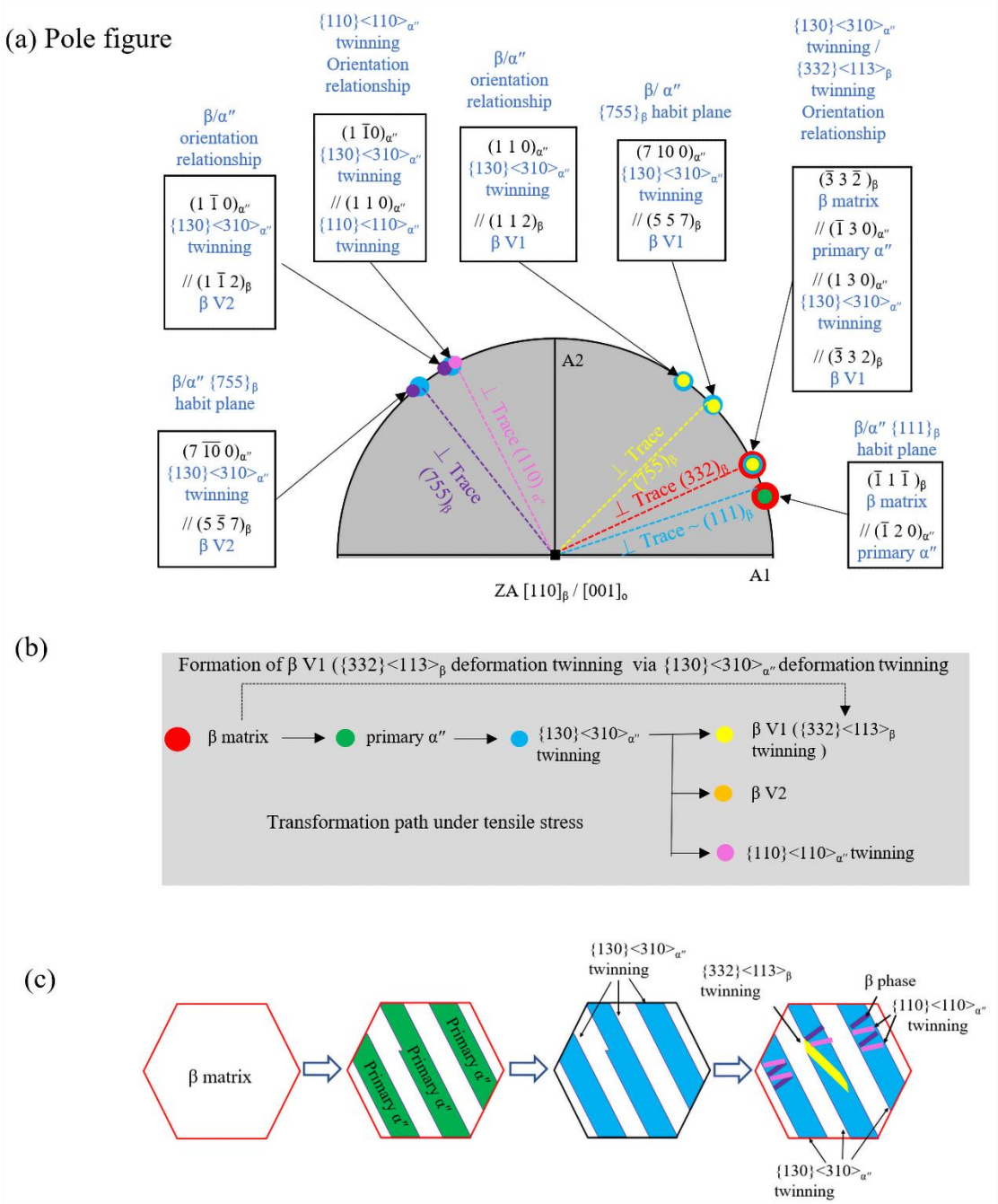

Figure 5 (a) The stereographic projections of the poles for all the deformation variants, identified in Figure 4 (orientation II) at the observation area along ZA $[110]_{\beta}$ / $[001]_{\alpha''}$. The orientation relationship and habit planes are indexed in the text blocks around the pole figure. The normal of the observed traces are plotted in the pole figure by dash lines; (b) and (c) transformation path under tensile stress. The $\{332\}<113>_{\beta}$ twinning relationship is identified between β matrix and β V1. The color code used in the Figure is the same one as in Figure 4.